Quantifying Local pH Changes in Carbonate Electrolyte during Copper-Catalysed CO_2 Electroreduction Using *In Operando* ^{13}C NMR

Michael Schatz[1,2,*], Sven Jovanovic[1], Rüdiger-A. Eichel[1,3], and Josef Granwehr[1,2]

[1]Institute of Energy and Climate Research, Fundamental Electrochemistry (IEK-9), Forschungszentrum Jülich, Jülich, 52425, Germany
[2]Institute of Technical and Macromolecular Chemistry, RWTH Aachen University, Aachen, 52074, Germany
[3]Institute of Physical Chemistry, RWTH Aachen University, Aachen, 52074, Germany
[*]m.schatz@fz-juelich.de

ABSTRACT

The electrochemical carbon dioxide reduction on copper attracted considerable attention within the last decade, since Cu is the only elemental transition metal that catalyses the formation of short-chain hydrocarbons and alcohols. Research in that field is mainly concentrated on understanding the reaction mechanism in terms of adsorbates and intermediates. Furthermore, dynamic changes in the microenvironment of the catalyst, *i.e.* local pH and CO_2 concentration values, play an equivalently decisive role in the selectivity of product formation. In this study, we present an *in operando* ^{13}C Nuclear Magnetic Resonance (NMR) technique that enables the simultaneous measurement of pH and CO_2 concentration in electrode vicinity during electroreduction. The influence of applied potential and buffer capacity of the electrolyte on the formation of formate is demonstrated. Herewith, theoretical considerations are confirmed experimentally and the importance of the interplay between catalyst and electrolyte is highlighted.

Introduction

In recent years, the electrochemical CO_2 reduction reaction (CO_2RR) has been recognized as a possible industrially applicable contribution for establishing a closed carbon cycle[1]. Driven by renewable electricity, this process has the potential to produce carbon-neutral fuels and feedstock chemicals while simultaneously stabilizing the electric grid by acting as energy store[2]. Among metal catalysts for CO_2RR, elemental copper has the exceptional ability to catalyse short-chain hydrocarbon evolution. In order to optimize future copper-based electrocatalyst designs, the understanding of underlying reaction mechanisms must be improved[3,4]. In addition to electrode surface characteristics and reaction conditions, the most influential factors for CO_2RR are properties of the aqueous solution surrounding the electrode, *i.e.* local pH and HCO_3^-/CO_2 concentration values[5–7]. How these local properties are affected by applied potential and how this in turn influences product formation has not been addressed experimentally owing to a lack of suitable *in operando* methods[8].

The first publication about Cu-catalysed CO_2RR by Hori *et al.*[3] discussed the interdependence of hydrocarbon and alcohol formation on local changes of the $KHCO_3$ buffer. In dilute $KHCO_3$ solution, the pH in cathode proximity will increase due to OH^- formation as part of the reduction reaction as well as poor buffer capacity of the solution. This in turn prevents Hydrogen Evolution Reaction (HER) and promotes the reduction of CO_2. If a potential more negative than $-1.1\,V$ vs. Normal Hydrogen Electrode is applied, CO stays adsorbed at the cathode and can be further reduced to C_{2+} products, e.g. ethylene, ethanol or even n-propanol[3]. Gupta *et al.* presented calculations investigating the interplay between local pH, buffer capacity and current density. For a bulk pH of 6.81 and a current density of $10\,A/m^2$, they determined a pH of up to 9 on the electrode surface. Due to the shifted CO_2/HCO_3^- equilibrium and simultaneous reduction of CO_2 in electrode proximity, a decrease of the local CO_2 concentration by a factor of 2.1 was predicted[9]. However, a decrease in CO_2 concentration does not translate linearly to a decrease in conversion rate. It has been shown using ^{13}C labelling that the main source of converted carbon is CO_2 from the equilibrium with HCO_3^-[10]. This led to the conclusion that the effective concentration of CO_2 in electrode vicinity is equivalent to the bulk[11]. Nonetheless, local CO_2 scarcity and basic pH dictate the reaction conditions at the electrode and must be considered for understanding the reaction mechanism of CO_2RR on copper.

Local pH effects have proven important in shifting the selectivity to desired products. A high local pH can be advantageous for reaction pathways that include a rate determining step without a proton transfer. In this case, hydrogen formation is hindered

while product formation is pH-independent. This applies *e.g.* to the C-C formation step in the reaction pathway to ethylene and ethanol[12–14]. In contrast, the formation of products that include a proton transfer in the rate determining step, e.g. methane, are inhibited[7]. Local shifts in the concentrations of CO_2 and HCO_3^- also affect the product formation: At small negative overpotential and therefore only modest changes in local pH, formate is formed in the presence of adsorbed CO_3^{2-}. More negative potentials shift the equilibrium to solution-based bicarbonate and promote CO formation[15,16].

The effect of local conditions have been utilized in electrode engineering. Roughened or porous electrode surfaces promote high local pH, which can effectively suppress HER[14] and simultaneously favour C_{2+} product formation by confinement of intermediate products[7,13]. However, a study using a Cu nanofoam electrode showed increased formate production over the whole potential range, suppressing the pathways to methane and ethylene almost completely[17]. This contradiction shows how important it is to understand the complex interplay between electrolyte composition, applied potential and surface morphology for electrode engineering. In order to generate a microenvironment that is suitable for the desired product formation, all of these parameters have to be considered[18]. Burdyny *et al.* even suggest considering the catalyst as combined surface and electrolyte system rather than just a metal surface[19]. To understand the catalytic performance of such a surface/electrolyte system, it is indispensable to know how local pH evolves during operation. Also, the CO_2 concentration and therefore the accessibility of the reactant varies locally.

Measuring local concentrations of protons and molecules that take part in electrochemical reactions has been attempted, for example, using scanning probe techniques and various optical methods.[20] Recent studies investigating CO_2RR apply Scanning Electrochemical Microscopy (SECM)[21], Surface-Enhanced Infrared Absorption Spectroscopy (SEIRAS)[22,23] and Surface-Enhanced Raman Spectroscopy (SERS)[24]. SECM offers direct measurement of the proton concentration by using the pH-sensitive electrochemical response of an inert metallic material. The SEIRAS and SERS methods measure the pH by monitoring the ratio of the species composing a buffer system and are, therefore, indirect measurement methods.[20]. In these experiments, typical buffer solutions for CO_2RR such as CO_2(aq)/HCO_3^-/CO_3^{2-}[21,22,24] and $H_2PO_4^-$/HPO_4^{2-}/PO_4^{3-}[23] were investigated.

In this study, the measurement of pH is demonstrated in an electrochemical cell and during CO_2 electrolysis by *in operando* ^{13}C Nuclear Magnetic Resonance (NMR), which has proven capable of investigating the CO_2(aq)/HCO_3^-/CO_3^{2-} equilibrium in such an environment[25]. In contrast to methods that only consider the CO_2(aq)/HCO_3^-[22] or the HCO_3^-/CO_3^{2-} equilibirum[24], the presented method provides data for a wide pH range by considering both equilibria, including an overlap region in-between. The sensitive volume of *in operando* NMR measurements is not limited to a few nanometres from the electrode like surface-enhanced optical methods and can provide spatial resolution when magnetic resonance imaging techniques are applied. Futhermore, NMR spectroscopy can provide a variety of additional information, e.g. sample chemistry, mobility and structure.

Electrochemical cells for *in operando* NMR measurements were developed and improved over the past 45 years[26–30], but high spectral resolution and sensitivity even in the presence of conductive material in the sensitive volume of the NMR setup has been demonstrated only recently. To calculate the pH from *in operando* ^{13}C NMR data, we utilize the buffer capability of HCO_3^-/CO_3^{2-}. Depending on the pH, either the equilibrium between HCO_3^- and H_2CO_3, or the equilibrium between HCO_3^- and CO_3^{2-} is dominant[5],

$$CO_3^{2-} + H^+ \rightleftharpoons HCO_3^-, \qquad pK_a = 10.3, \tag{1}$$

$$HCO_3^- + H^+ \rightleftharpoons H_2CO_3 \quad \left(\rightleftharpoons CO_2(aq) + H_2O\right), \qquad pK_a = 6.4. \tag{2}$$

Moret *et al.* have shown that due to the fast exchange between HCO_3^- and CO_3^{2-} compared to the NMR time scale given by the chemical shift difference, the ^{13}C resonances coalesce into a single peak with a pH dependent chemical shift. Hence, the term 'carbonate' is used in the following to describe both HCO_3^- and CO_3^{2-} in solution. The respective molecular formula is used when referring to a specific species. Alternatively, Scholz *et al.* estimated the pH in near neutral conditions using the Hendersson–Hasselbalch (HH) equation[31],

$$pH = pK_a + \log_{10}\frac{[HCO_3^-]}{[CO_2]}. \tag{3}$$

Here, both methods are combined to assess the possibility of pH measurements over a wide range from neutral to basic environments. This technique is then applied *in operando* by varying potential and electrolyte concentration for a comparison with theoretical predictions, and to obtain new insights about the interplay with local pH, CO_2 accessibility, and buffer capacity.

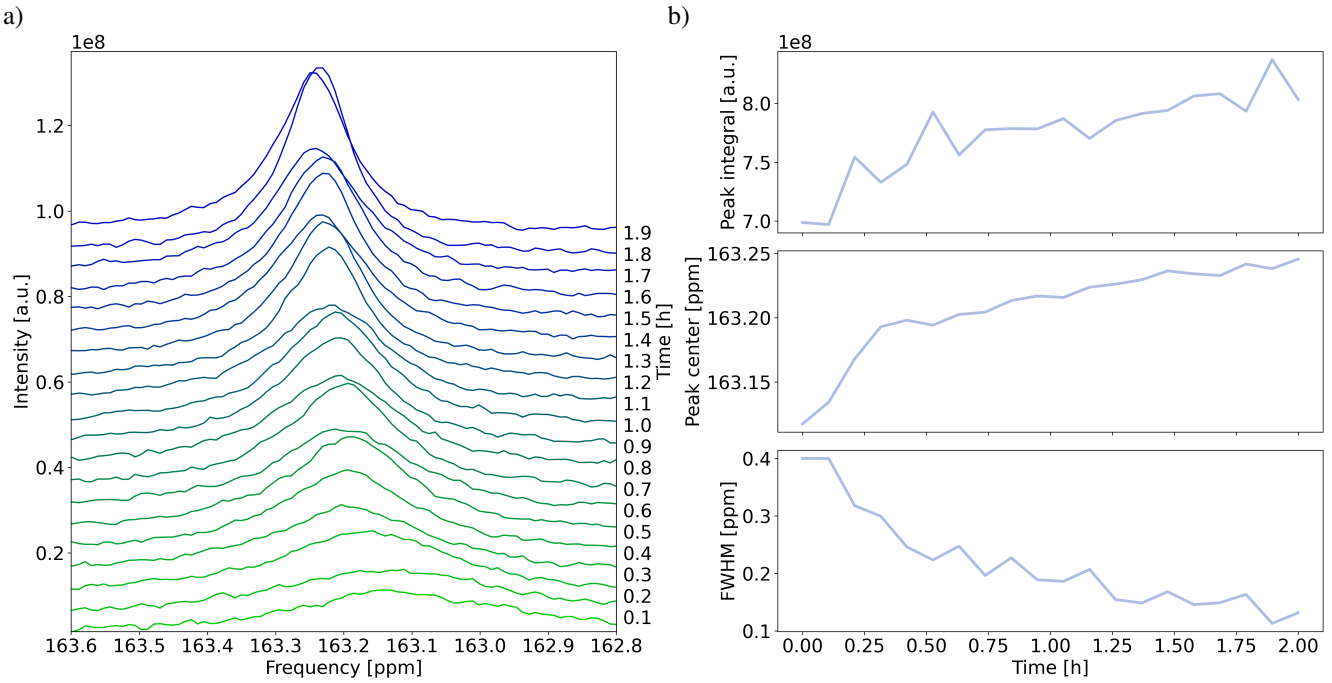

Figure 1. ^{13}C NMR resonance of carbonate during electrolysis at −1.47 V, with an initial $KHCO_3$ concentration of 0.1 M. a) Evolution of the carbonate peak during 2 h of electrolysis. b) Temporal evolution of the integral (top), ^{13}C chemical shift (middle), and FWHM (bottom) of the Lorentzian function fitted to the carbonate peak. Further data representing experiments at different potentials and concentrations are shown in Figure S3 and S4.

Results and discussion

In the ^{13}C NMR spectra, the three observed singlet peaks are assigned to the ^{13}C-labelled methyl carbon of acetonitrile, to CO_2, and to a coalesced resonance of HCO_3^- and CO_3^{2-} due to the fast exchange between these species. The peak properties of the three ^{13}C signals, *i.e.* integral, position (chemical shift) and full width at half maximum (FWHM), were determined by peak fitting using a Lorentzian function, which provided an adequate fit. For error estimation, fluctuations of the fitted values are determined in terms of standard deviation using a 5-step moving average. Details about the error estimation are available in Section S2 and Figure S6 in the Supporting Information. Figure 1a shows the ^{13}C resonance of carbonate at −1.47 V as a function of time, with an initial $KHCO_3$ concentration of 0.1 M. The evolution of the fitted peak properties is shown in Figure 1b. The carbonate chemical shift (CCS) moves downfield from an initial value of 163.12 ppm, while the integral of the carbonate peak increases. This constitutes a shift of the HCO_3^-/CO_2 equilibrium towards HCO_3^-, caused by an increasing local pH. The FWHM decreases due to faster exchange between carbonate species, which has been observed before by *in operando* NMR studies with silver working electrodes[25]. The fitting parameters exhibit fluctuations that can be attributed to gas bubble formation on the electrode during the electrochemical experiments. The magnetic susceptibility of gas bubbles differs significantly from the surrounding electrolyte, causing inhomogeneities in the magnetic field that are perceived as variations of the peak shape. Furthermore, the quality factor of the resonant circuit used for radio frequency excitation and detection changes, leading to an additional fluctuation of the integral. The fluctuations of the peak parameters relative to the total CCS change during the experiment are $(11.6 \pm 4.6)\,\%$ for CCS, and $(11.4 \pm 3.4)\,\%$ for the FWHM. The fluctuations of the integral relative to its initial value is $(3.6 \pm 0.6)\,\%$.

The integral of the CO_2 resonance at 127.5 ppm decreases, approaching zero during experiments with high negative potential. Chemical shift and width stay constant. This is expected and confirms that the origin of the aforementioned carbonate resonance shift is a variation of the HCO_3^-/CO_2 equilibrium.

Acetonitrile as reference substance is isolated by a glass capillary and consequently does not interact with other species during electrolysis. Hence, chemical shift, integral and width of its ^{13}C-labelled methyl group are unaffected by the electrolysis reaction itself. Still, the formation of gas bubbles leads to fluctuations of the line shape. Fluctuations of chemical shift and FWHM relative to the total change in CCS are $(11.61 \pm 4.2)\,\%$ and $(22.6 \pm 4.7)\,\%$, respectively. If these fluctuations were a result of temperature fluctuations of the sample, the former would correspond to a negligible changes in temperature of 0.1 °C.

To calculate the local pH from the evolution of the carbonate chemical shift δ_c, a reference curve for the pH-dependence

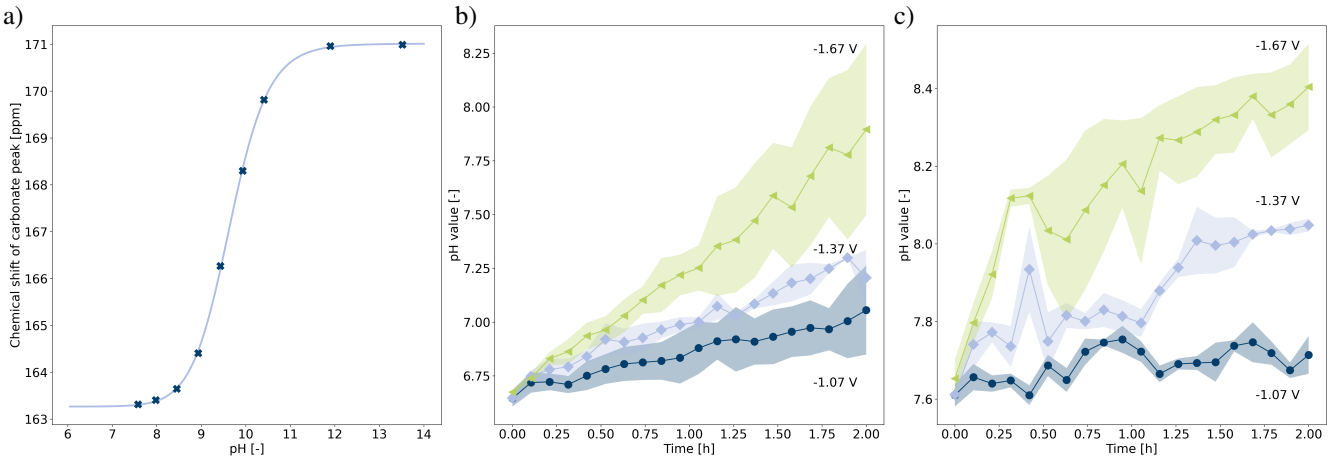

Figure 2. pH calculation using the CCS for pH $\geq$ 7.6 and the HH equation for pH $<$ 7.6. a) pH dependent CCS at 10 °C. Data points are marked by crosses and the fitted sigmoidal function by a solid line. b-c) pH values as a function of time for initial electrolyte concentration of 0.1 M (b) and 1 M (c). Data points represent average value of experiments with an applied potential of −1.07 V (dark blue), −1.37 V (light blue) and −1.67 V (green). Coloured areas show minimum and maximum value of the respective data point. Further data representing experiments at other potentials are available in Figure S5.

was recorded by titration of a 1 M $KHCO_3$ solution with 1 M KOH, which resulted in a typical sigmoidal curve depicted in Figure 2a that was fitted by

$$\delta_c = \delta_{HCO_3^-} + \frac{\delta_{CO_3^{2-}} - \delta_{HCO_3^-}}{1 + 10^{pK_a - pH}}. \tag{4}$$

This function is derived from the carbonate equilibrium (see Section S1 of the Supporting Information). The fitted parameters are $\delta_{HCO_3^-=163.27\,ppm}$, $\delta_{CO_3^{2-}=171.01\,ppm}$ and $pK_a = 9.64$. Equation 4 can be transformed to obtain an expression for the pH value,

$$pH = pK_a + \log_{10}\left|\frac{\delta_c - \delta_{HCO_3^-}}{\delta_c - \delta_{CO_3^{2-}}}\right|. \tag{5}$$

Using the titration curve, a lower threshold of pH = 7.6 for reliable pH estimation by means of the CCS was obtained. Below this threshold, changes of the CCS are small compared to the measurement accuracy, and the equilibrium between CO_2 and HCO_3^- is dominant. Therefore, the HH equation 3 is more accurate for the determination of the pH value below pH = 7.6. Here, the ratio of the integrals of CO_2 and carbonate peak can be used equivalently to the ratio of the concentrations of the respective species[31].

The pK_a values vary from literature data, since experiments are carried out at 10 °C. Other influencing factors are the ionic strength of the electrolyte and the CO_2 concentration in the gas phase. Thus, the pK_a of equation 2 is determined experimentally using the HH equation 3 and the initial pH value in the NMR tube, which was measured with a pH meter before the experiment. Averaged over the whole data set, this resulted in a calculated pK_a of 6.15 ± 0.06 and 6.02 ± 0.07 for the 0.1 M and 1 M experiments, respectively.

Figure 2b and 2c show the measured pH versus time for $KHCO_3$ concentrations of 0.1 M and 1 M, respectively, and for three representative potentials. A more negative potential results in an accelerated pH increase in both cases. In 0.1 M solution the increase is almost linear, while in 1 M solution a fast increase is observed at the beginning of the experiment, followed by a deceleration of this development. In curves that pass the threshold of pH 7.6 no discontinuity is found, which indicates that the used methods are compatible. For experiments with an initial $KHCO_3$ concentration of 0.1 M, the measured pH was mainly below the threshold pH 7.6. The data range shown in Figure 2b is therefore larger than in 2c, where primarily the CCS function was used for pH determination. These increased fluctuations are explained by a larger impact of bubble formation on signal integrals compared to the effect on chemical shifts. For the highest applied potential, the highest rate of bubble formation is observed, which results in increased uncertainties in the pH value for both electrolyte concentrations.

The evolution of the pH value is in accordance with pH values measured before and after electrolysis using a pH meter, *cf.* Figure S7. All curves start at the expected pH value for CO_2 saturated $KHCO_3$ solution, *i.e.* at pH 6.7 for 0.1 M and at pH

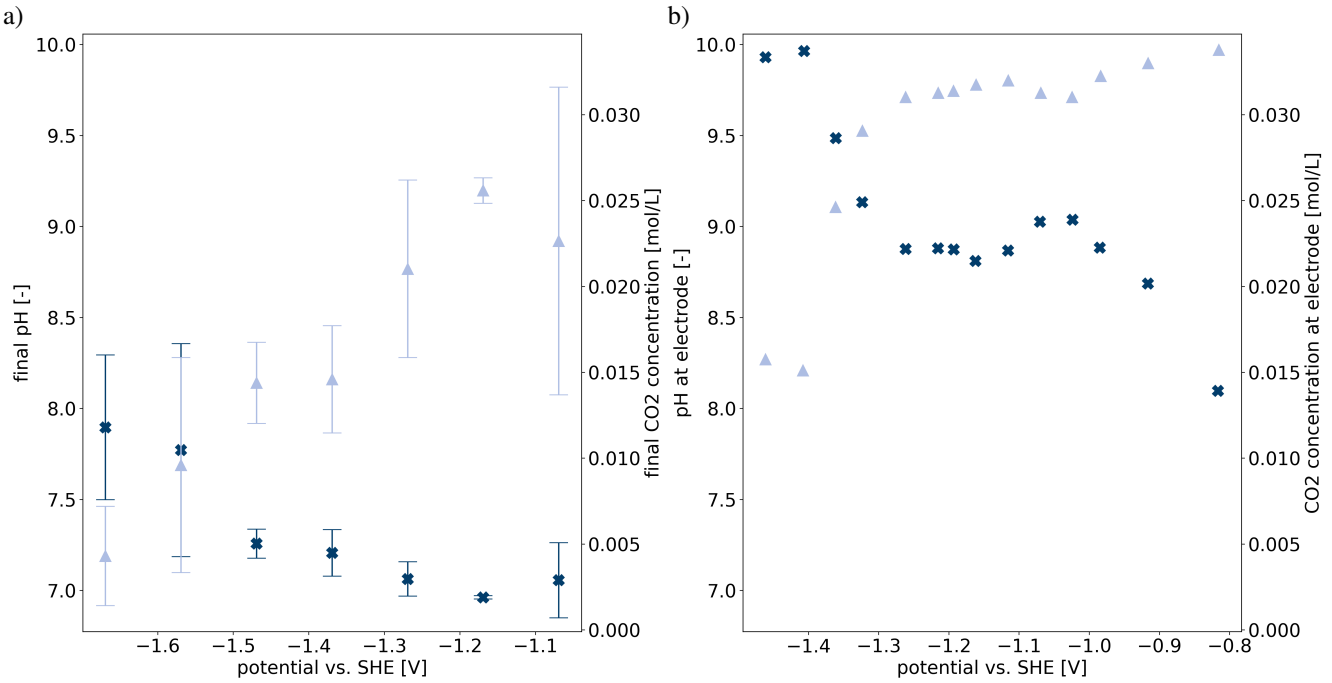

Figure 3. Comparison of experimental and theoretical potential-dependent pH and CO_2 concentration. a) pH (×) and CO_2 concentration (△) values determined by ^{13}C NMR at the end of a potential step, recorded at potentials between −1.07 V and −1.67 V; b) Calculated pH (×) and CO_2 concentration (△) at the electrode. Values are taken from Figure 8 in Gupta *et al.*[9]. Since final values of the statistical average over a volume surrounding the electrode from a batch experiment are compared with steady state values in direct electrode proximity from a computer calculation, this depiction serves as a qualitative comparison.

7.6 for 1 M. Final pH values at the end of the electrolysis experiment are larger than the values measured with the pH meter. This could be a manifestation of non-equilibrium between carbon species in solution and CO_2 in the atmosphere caused by electrolysis, or it could be a local pH effect. Since the liquid–gas interface in the NMR tube is small and the distance between the surface and the WE is sizeable, $CO_2(g) \leftrightarrow CO_2(aq)$ exchange as well as CO_2 diffusion may not be fast enough to keep the electrolyte at the WE, which is in the sensitive volume for the NMR, in a quasi-equilibrium. After operation, the concentration equilibrates between gas and liquid phase as well as between bulk and electrolyte in the sensitive NMR volume and, therefore, the pH measured by the pH meter after electrolysis is lower than the final pH measured by *in operando* NMR. The NMR measurements represent a statistical average over the whole NMR sensitive volume around the electrode, which means that even higher pH near the electrode surface could be expected. Since the line width of the carbonate peak is small, no spatial distribution of pH is indicated. Therefore, the equilibration of the pH value inside the sensitive NMR volume is faster than the change of the pH. Such an equilibration would not be expected on the time scale of the experiment if only self-diffusion in aqueous media are considered. It may be facilitated by diffusion caused by a concentration gradient due to electrolysis at the electrode, or by convection due to Joule heating. Only minor temperature differences can cause sufficient motion in the sample to achieve such an averaging at the employed low current densities. At the same time, as postulated by Varela *et al.* the local pH of a dilute $KHCO_3$ solution might even exhibit the local pH of a more concentrated solution[32]. The data in Figure 2b and 2c show larger difference between measured and initial pH for the more dilute solution, thus confirming this hypothesis.

The potential-dependent local pH effect can be qualitatively compared to the calculations by Gupta *et al.*[9]. Figure 3a depicts the final pH value determined by *in operando* NMR as a measure for the pH in the vicinity of the electrode as well as the final CO_2 concentration, which was determined assuming a saturation concentration of 52.7 mM at 10 °C[25]. Final pH values and CO_2 concentrations show a opposing course, *i.e.* low pH and high CO_2 concentration for low potentials and vice versa for high potentials. A plateau between −1.1 V and −1.4 V is followed by an abrupt increase in pH and therefore decrease in CO_2 concentration at more negative potential. This course can also be observed in the data of Gupta *et al.*, shifted by approximately 100 mV to higher potentials, as depicted in Figure 3b. Such a shift may be caused by the absence of an iR drop in the theoretical study. Katsounaras *et al.* attribute this plateau to inhibition of the HER in the specific local pH region resulting from the applied potentials[33].

After electrolysis, the electrodes are removed from the electrolyte. The liquid solution is then analysed *ex situ* to detect

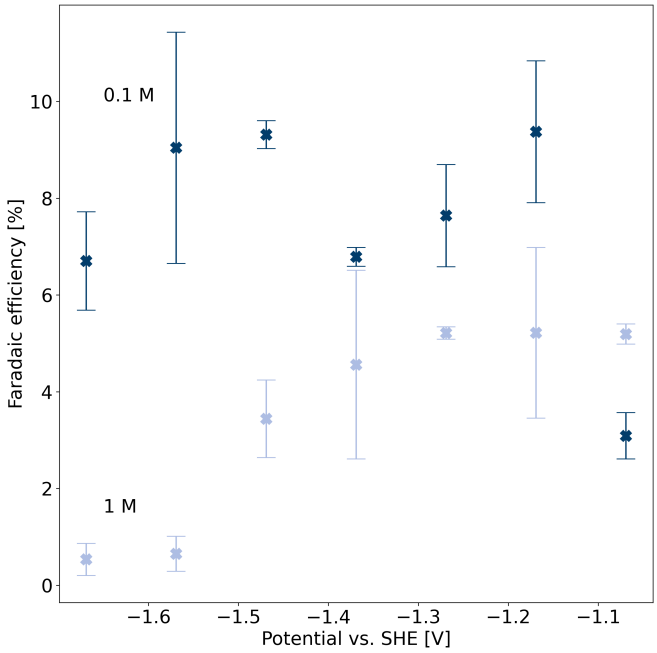

Figure 4. Potential-dependent Faradaic efficiencies of formate production in 1 M and 0.1 M $KHCO_3$ solution.

liquid products that have formed during electrolysis. The reference compound TSP is added in 1 mM concentration and the sample is investigated by ^{1}H NMR with water suppression at a magnetic field of 18.8 T (800 MHz for ^{1}H). Formate is the major liquid product in Cu-catalysed CO_2RR at the employed current densities[4]. Other ^{13}C-labelled molecules could not be identified in our experiments, *cf.* Figure S8 for the ^{1}H spectra. Low selectivity for these products, a polycrystalline and untreated Cu surface, or even contamination by Ag^+ ions from the reference electrode could be possible reasons[34]. However, potential-dependent Faradaic Efficiencies (FE) of formate, depicted in Figure 4, show varying selectivity for this reaction pathway for the initial carbonate concentrations in consideration. The reaction pathway to formate is a "dead-end road", as it is not further reduced on a Cu electrode[5], although others suggest a possible pathway to methanol[35]. However, it competes with the pathway to CO and its further reduced products, *i.e.* methane, ethylene and other short-chain hydrocarbons. Therefore, the formation of formate is used to distinguish the favoured reaction pathway under varying conditions[36]. In general, FE for formate is lower over the whole potential range for the more concentrated solution. At high potentials, the FE approaches zero. This is expected, as at high potential and/or strongly basic local conditions formate formation was found to be suppressed by a shift from adsorbed to solution-based bicarbonate[16]. This effect is less pronounced in 0.1 M solution as the pH value at the beginning of the experiment is low. Towards the end of the experiment the increase in local pH inhibits formate formation. In the investigated potential range, the formate formation in the diluted solution is therefore almost potential-independent. The strong suppression of formate formation at the most negative potentials is also due to the dynamic changes of surface pH: Figure 2c shows a rapid increase in local pH in the first minutes of operation inhibiting any further formate formation during electrolysis.

Conclusion

In conclusion, this work presents a proof of principle for *in operando* determination of pH in electrode proximity in a bicarbonate/carbonate buffer system using ^{13}C NMR spectroscopy. In a pH range between approximately 4 to 12, the calculation using a combination of titration curve of the carbonate chemical shift and Hendersson–Hasselbalch equation has proven to be robust even when the system is disturbed by the formation of gas bubbles. The potential dependent changes of local pH and CO_2 concentration are in qualitative accordance with simulated data from literature. The experiments demonstrate a significant increase in local pH, emphasizing that the bulk pH can not be assumed as a valid reaction condition in direct electrode vicinity. Dilute electrolytes with a low bulk pH but also low buffer capacity might even result in higher local pH than found in a concentrated electrolyte. *Ex situ* product analysis showed that the selectivity for formate is dependent on the local pH rather than potential-dependent in the investigated potential range. This work presents a method that can be easily applied to a wide range of electrode materials and can facilitate the determination of real reaction conditions in terms of local pH and

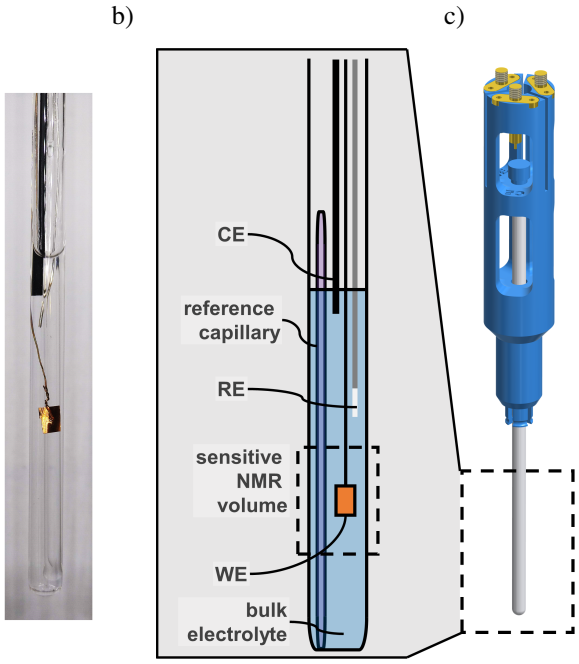

Figure 5. Electrochemical cell for *in operando* ^{13}C NMR. a) Photograph and b) schematic of the cell, including copper working electrode (WE), chlorinated silver wire reference electrode (RE), graphite rod counter electrode (CE), and reference capillary. c) Model of the 3D printed sample holder fitting onto the NMR probe.

CO_2 concentration.

Methods

The *in operando* electrolysis cell and the shielding setup were constructed as described previously[25]. In the following, only changes in the cell setup and the experimental procedure are mentioned.

Electrochemical cell

Copper foil (GoodFellow GmbH, Hamburg, Germany) with outer dimensions of 2.5 mm × 4 mm × 0.05 mm is perforated and the stripped end of a copper wire (GoodFellow GmbH, Hamburg, Germany) with 0.15 mm diameter and 0.025 mm PTFE insulation is pulled through the hole and twisted around itself to ensure contacting. For every experiment a new working electrode is used. Other electrodes are rinsed with demineralized water and reused. A capillary containing ^{13}C-labelled acetonitrile (99 atom %, $^{13}CH_3{}^{12}CN$, Sigma Aldrich, Munich, Germany) was introduced into the cell as an external NMR reference. The liquid was pulled into a 50 µL capillary pipette (Hirschmann Laborgeräte GmbH & Co. KG, Eberstadt, Germany) by capillary forces before melting both ends of the capillary. The closed capillary was placed into the NMR tube in a way that the reference liquid is equally distributed in the sensitive volume of the probehead. The reference substance did not only serve as a chemical shift reference, with a ^{13}C chemical shift of 4.43 ppm *vs.* trimethylsilylpropanoic acid (TSP) at 10 °C, but it could also be used to correct for amplitude fluctuations and phase drifts that may be caused by variations of the tuning mode during an experiment. Qualitatively, it indicated line shape changes induced by bubbles as well, but since these changes are different for the electrolyte and the reference sample, a correction is challenging and has not been attempted. The temperature-dependent ^{13}C chemical shift of $^{13}CH_3{}^{12}CN$, δ_{CH_3CN}, referenced to trimethylsilylpropanoic acid (TSP) is depicted in Figure S1. The linear correlation is used to estimate temperature gradients in the sample due to radio frequency excitation,

$$\delta_{CH_3CN} = -0.0104\,\frac{\text{ppm}}{^\circ\text{C}} \times T + 4.5308\,\text{ppm}, \tag{6}$$

where T is the temperature in °C. A schematic of the electrochemical cell and the full assembly is depicted in Figure 5.

Electrolyte preparation

^{13}C-enriched stock solutions of $KHCO_3$ (98 atom %, Sigma Aldrich Chemie GmbH, Munich, Germany) were prepared at 0.1 M and 1 M concentrations and pre-electrolysed as described by Hori *et al.*[37] in order to remove impurities such as heavy

metal ions, which will otherwise negatively affect the performance of the electrolysis. 20 mL of the respective stock solution were filled into a twin-necked flask connected to a Schlenk line and degassed by three freeze-pump-thaw cycles. Using two 5 mm × 5 mm platinum mesh electrodes (GoodFellow GmbH, Hamburg, Germany) a constant current of 150 µA was applied for 20 h while stirring with ca. 250 rpm using a magnetic stirrer. 600 µL of stock solution were filled in a NMR tube and bubbled until saturation for ca. 20 min at a flow rate of ca. 0.3 mL s^{-1} in a water bath at 10 °C with ^{13}C-enriched CO_2 (99 atom %, Sigma Aldrich, Munich, Germany). The pH value was measured after CO_2 saturation and later after electrolysis using a benchtop Mettler–Toledo FiveEasy pH meter with a Mettler–Toledo InLab NMR pH electrode (Mettler–Toledo GmbH, Giessen, Germany) for direct pH measurement of the sample in the NMR tube. The three-electrode setup including the reference capillary was introduced afterwards into the NMR tube and the tube sealed with a gas tight cap. The NMR tube was mounted in a 3D-printed holder that fits onto the NMR probe and provides connectors for the electrodes to the potentiostat. The probe was pre-tempered at 10 °C to avoid degassing due to transient temperature effects during thermal equilibration.

Electrochemical parameters

The electrodes of the electrochemical cell were connected to a BioLogic SP-200 potentiostat (BioLogic Science Instruments, Seyssinet-Pariset, France). The employed micro reference electrode exhibited a steady open circuit voltage (OCV) of 0.115 ± 0.002 V *vs.* a commercial Ag/AgCl (3 M KCl) reference electrode (Deutsche METROHM GmbH & Co. KG, Filderstadt, Germany) in a 1 M $KHCO_3$ solution. All potentials are converted to the Standard Hydrogen Electrode (SHE) scale according to

$$E_{\mathrm{SHE}} = E_{\mathrm{microAg/AgCl}} + 0.205\,\mathrm{V} - 0.73 \times 10^{-3}\,\mathrm{V/K} \times (T - 298.15\,\mathrm{K}) + 0.115\,\mathrm{V}\,, \tag{7}$$

where T is the temperature in K[38]. Chronoamperometric (CA) measurements were conducted for 2 hours at constant potential, with seven data points in the range of $[-1.67\,\mathrm{V}, -1.07\,\mathrm{V}]$ vs. SHE and two repetitions. Results of CA measurements in 0.1 M and 1 M solutions are depicted in Figure S2. Figure S2a and S2b show that bubble formation has an effect on the evolution of current density as well, which exhibits increasing fluctuations with more negative potential.

NMR parameters

The cell was inserted into the broadband gradient probehead DiffBB of a Bruker Avance III HD spectrometer (Bruker BioSpin GmbH, Rheinstetten, Germany) with a 9.4 T wide-bore magnet, corresponding to a ^{13}C resonance frequency of 100.6 MHz. The cell holder presented in our previous publication[25] was adjusted such that the cell can be inserted from the top of the magnet with a narrow-bore sample lift installed. During CA, ^{13}C spectra were continuously recorded using 30°-pulses with ^{1}H decoupling (WALTZ-16 sequence with 128 repetitions every 2 s), resulting in acquisition of one spectrum every 6 min. A pulse length of 4 µs and a radio frequency power of 40.996 W was set. Spectra were processed with 1 Hz line broadening and zero-filling.

After the *in operando* experiment, electrodes and reference capillary were removed from the tube and the sample was analysed *ex situ* to study the formation of liquid products. To enable quantification, a well-defined amount of the reference substance TSP was added to the sample, so that it results in a concentration of 1 mM. For higher sensitivity, ^{1}H NMR with water suppression using excitation sculpting with perfect echo was performed[39]. In addition, the sample was analysed at higher magnetic field of 18.8 T (800 MHz for ^{1}H) using a Bruker DiffBB probehead. The relaxation delay was set to 5 s, and 256 scans were acquired. The pulse length was 21 µs and the pulse power was 27.58 W. The pulse length of the sine-shaped selective pulse was 800 µs and the respective pulse power was 0.21943 W. Resulting ^{1}H spectra are depicted in Figure S8, showing the formate resonance doublet at 8.46 ppm. The Faradaic Efficiency (FE) of formate was calculated according to

$$\mathrm{FE} = \frac{S_{\mathrm{formate}}}{S_{\mathrm{TSP}}} \times 9 \times 2 \times 1\,\mathrm{mM} \times 600\,\mu\mathrm{L} \times \frac{F}{\int_0^{2\,\mathrm{h}} I_{\mathrm{CA}}(t)\,dt}, \tag{8}$$

where S_{formate} and S_{TSP} are the integral of the peaks of formate and TSP, respectively, F is the Faraday constant and $I_{\mathrm{CA}}(t)$ is the current as a function of time during the CA experiment. The factor 9 in equation 8 results from the quotient of protons of TSP and formate, and the factor 2 represents the number of electron transferred per formate molecule formed.

References

1. Masel, R. I. *et al.* An industrial perspective on catalysts for low-temperature co2 electrolysis. *Nat. nanotechnology* DOI: 10.1038/s41565-020-00823-x (2021).

2. Grim, R. G. *et al.* Transforming the carbon economy: challenges and opportunities in the convergence of low-cost electricity and reductive co 2 utilization. *Energy & Environ. Sci.* **13**, 472–494, DOI: 10.1039/C9EE02410G (2020).

3. Hori, Y., Murata, A. & Takahashi, R. Formation of hydrocarbons in the electrochemical reduction of carbon dioxide at a copper electrode in aqueous solution. *J. Chem. Soc. Faraday Transactions 1: Phys. Chem. Condens. Phases* **85**, 2309, DOI: 10.1039/f19898502309 (1989).

4. Kuhl, K. P., Cave, E. R., Abram, D. N. & Jaramillo, T. F. New insights into the electrochemical reduction of carbon dioxide on metallic copper surfaces. *Energy & Environ. Sci.* **5**, 7050, DOI: 10.1039/c2ee21234j (2012).

5. Gattrell, M., Gupta, N. & Co, A. A review of the aqueous electrochemical reduction of co2 to hydrocarbons at copper. *J. Electroanal. Chem.* **594**, 1–19, DOI: 10.1016/j.jelechem.2006.05.013 (2006).

6. Peterson, A. A., Abild-Pedersen, F., Studt, F., Rossmeisl, J. & Nørskov, J. K. How copper catalyzes the electroreduction of carbon dioxide into hydrocarbon fuels. *Energy & Environ. Sci.* **3**, 1311, DOI: 10.1039/c0ee00071j (2010).

7. Sa, Y. J. *et al.* Catalyst-electrolyte interface chemistry for electrochemical co2 reduction. *Chem. Soc. reviews* **49**, 6632–6665, DOI: 10.1039/d0cs00030b (2020).

8. Mustafa, A. *et al.* Theoretical insights into the factors affecting the electrochemical reduction of co 2. *Sustain. Energy & Fuels* **4**, 4352–4369, DOI: 10.1039/D0SE00544D (2020).

9. Gupta, N., Gattrell, M. & MacDougall, B. Calculation for the cathode surface concentrations in the electrochemical reduction of co2 in khco3 solutions. *J. Appl. Electrochem.* **36**, 161–172, DOI: 10.1007/s10800-005-9058-y (2006).

10. Zhu, S., Jiang, B., Cai, W.-B. & Shao, M. Direct observation on reaction intermediates and the role of bicarbonate anions in co2 electrochemical reduction reaction on cu surfaces. *J. Am. Chem. Soc.* **139**, 15664–15667, DOI: 10.1021/jacs.7b10462 (2017).

11. Dunwell, M. *et al.* Examination of near-electrode concentration gradients and kinetic impacts on the electrochemical reduction of co 2 using surface-enhanced infrared spectroscopy. *ACS Catal.* **8**, 3999–4008, DOI: 10.1021/acscatal.8b01032 (2018).

12. Resasco, J., Lum, Y., Clark, E., Zeledon, J. Z. & Bell, A. T. Effects of anion identity and concentration on electrochemical reduction of co 2. *ChemElectroChem* **5**, 1064–1072, DOI: 10.1002/celc.201701316 (2018).

13. Handoko, A. D. *et al.* Mechanistic insights into the selective electroreduction of carbon dioxide to ethylene on cu 2 o-derived copper catalysts. *The J. Phys. Chem. C* **120**, 20058–20067, DOI: 10.1021/acs.jpcc.6b07128 (2016).

14. Hall, A. S., Yoon, Y., Wuttig, A. & Surendranath, Y. Mesostructure-induced selectivity in co2 reduction catalysis. *J. Am. Chem. Soc.* **137**, 14834–14837, DOI: 10.1021/jacs.5b08259 (2015).

15. Dunwell, M. *et al.* The central role of bicarbonate in the electrochemical reduction of carbon dioxide on gold. *J. Am. Chem. Soc.* **139**, 3774–3783, DOI: 10.1021/jacs.6b13287 (2017).

16. Moradzaman, M. & Mul, G. Infrared analysis of interfacial phenomena during electrochemical reduction of co 2 over polycrystalline copper electrodes. *ACS Catal.* **10**, 8049–8057, DOI: 10.1021/acscatal.0c02130 (2020).

17. Sen, S., Liu, D. & Palmore, G. T. R. Electrochemical reduction of co 2 at copper nanofoams. *ACS Catal.* **4**, 3091–3095, DOI: 10.1021/cs500522g (2014).

18. Weitzner, S. E. *et al.* Toward engineering of solution microenvironments for the co2 reduction reaction: Unraveling ph and voltage effects from a combined density-functional-continuum theory. *The J. Phys. Chem. Lett.* **11**, 4113–4118, DOI: 10.1021/acs.jpclett.0c00957 (2020).

19. Burdyny, T. & Smith, W. A. Co 2 reduction on gas-diffusion electrodes and why catalytic performance must be assessed at commercially-relevant conditions. *Energy & Environ. Sci.* **12**, 1442–1453, DOI: 10.1039/c8ee03134g (2019).

20. Monteiro, M. C. & Koper, M. T. Measuring local ph in electrochemistry. *Curr. Opin. Electrochem.* **25**, 100649, DOI: 10.1016/j.coelec.2020.100649 (2021).

21. Monteiro, M. C. O. *et al.* Time-resolved local ph measurements during co2 reduction using scanning electrochemical microscopy: Buffering and tip effects. *JACS Au* **1**, 1915–1924, DOI: 10.1021/jacsau.1c00289 (2021).

22. Ayemoba, O. & Cuesta, A. Spectroscopic evidence of size-dependent buffering of interfacial ph by cation hydrolysis during co2 electroreduction. *ACS Appl. Mater. & Interfaces* **9**, 27377–27382, DOI: 10.1021/acsami.7b07351 (2017).

23. Yang, K., Kas, R. & Smith, W. A. In situ infrared spectroscopy reveals persistent alkalinity near electrode surfaces during co2 electroreduction. *J. Am. Chem. Soc.* **141**, 15891–15900, DOI: 10.1021/jacs.9b07000 (2019).

24. Henckel, D. A. *et al.* Potential dependence of the local ph in a co 2 reduction electrolyzer. *ACS Catal.* **11**, 255–263, DOI: 10.1021/acscatal.0c04297 (2021).

25. Jovanovic, S. *et al.* An electrochemical cell for in operando 13c nuclear magnetic resonance investigations of carbon dioxide/carbonate processes in aqueous solution. *Magn. Reson.* **2**, 265–280, DOI: 10.5194/mr-2-265-2021 (2021).

26. Richards, J. A. & Evans, D. H. Flow cell for electrolysis within the probe of a nuclear magnetic resonance spectrometer. *Anal. Chem.* **47**, 964–966, DOI: 10.1021/ac60356a016 (1975).

27. Webster, R. D. In situ electrochemical-nmr spectroscopy. reduction of aromatic halides. *Anal. Chem.* **76**, 1603–1610, DOI: 10.1021/ac0351724 (2004).

28. Klod, S., Ziegs, F. & Dunsch, L. In situ nmr spectroelectrochemistry of higher sensitivity by large scale electrodes. *Anal. Chem.* **81**, 10262–10267, DOI: 10.1021/ac901641m (2009).

29. Bussy, U. *et al.* In situ nmr spectroelectrochemistry for the structure elucidation of unstable intermediate metabolites. *Anal. Bioanal. Chem.* **405**, 5817–5824, DOI: 10.1007/s00216-013-6977-z (2013).

30. Pietrzak, M. *et al.* Recent progress in liquid state electrochemistry coupled with nmr spectroscopy. *ChemElectroChem* **8**, 4181–4198, DOI: 10.1002/celc.202100724 (2021).

31. Scholz, D. J. *et al.* Quantified ph imaging with hyperpolarized (13) c-bicarbonate. *Magn. resonance medicine* **73**, 2274–2282, DOI: 10.1002/mrm.25357 (2015).

32. Varela, A. S., Kroschel, M., Reier, T. & Strasser, P. Controlling the selectivity of co2 electroreduction on copper: The effect of the electrolyte concentration and the importance of the local ph. *Catal. Today* **260**, 8–13, DOI: 10.1016/j.cattod.2015.06.009 (2016).

33. Katsounaros, I. *et al.* The effective surface ph during reactions at the solid–liquid interface. *Electrochem. Commun.* **13**, 634–637, DOI: 10.1016/j.elecom.2011.03.032 (2011).

34. Leung, K. Y. & McCrory, C. C. L. Effect and prevention of trace ag + contamination from ag/agcl reference electrodes on co 2 reduction product distributions at polycrystalline copper electrodes. *ACS Appl. Energy Mater.* **2**, 8283–8293, DOI: 10.1021/acsaem.9b01759 (2019).

35. Albo, J., Alvarez-Guerra, M., Castaño, P. & Irabien, A. Towards the electrochemical conversion of carbon dioxide into methanol. *Green Chem.* **17**, 2304–2324, DOI: 10.1039/C4GC02453B (2015).

36. Nguyen, T. N. *et al.* Electrochemical co 2 reduction to ethanol: from mechanistic understanding to catalyst design. *J. Mater. Chem. A* DOI: 10.1039/D1TA01115D (2021).

37. Hori, Y. *et al.* "deactivation of copper electrode" in electrochemical reduction of co2. *Electrochimica Acta* **50**, 5354–5369, DOI: 10.1016/j.electacta.2005.03.015 (2005).

38. Sawyer, D. T., Sobkowiak, A. & Roberts, J. L. *Electrochemistry for chemists* (Wiley, New York, 1995), 2. ed. edn.

39. Adams, R. W., Holroyd, C. M., Aguilar, J. A., Nilsson, M. & Morris, G. A. "perfecting" watergate: clean proton nmr spectra from aqueous solution. *Chem. Commun.* **49**, 358–360, DOI: 10.1039/c2cc37579f (2013).

Acknowledgements

The authors thank Emmanouil Veroutis and P. Philipp M. Schleker for technical assistance and fruitful discussions. This research has been supported by the German Research Foundation (DFG) under Germany's Excellence Strategy – Cluster of Excellence 2186 "The Fuel Science Center" (grant no. 390919832).

Author contributions statement

M.S. and S.J. developed the experimental procedure. M.S. conducted the experimental work and processed the data. M.S., S.J., J.G. interpreted the results. R.-A. E. and J.G. supervised the project. M.S. wrote the manuscript. All authors reviewed the manuscript.

Additional information

Supplementary information is available for this paper.
Competing Interests: The authors declare that they have no competing interests.
Correspondence and requests for materials should be addressed to M.S.